

The inverse electromagnetic shaping problem

Alfredo Canelas · Jean R. Roche · José Herskovits

Received: 12 February 2008 / Revised: 28 May 2008 / Accepted: 8 June 2008 / Published online: 22 July 2008
© Springer-Verlag 2008

Abstract The inverse problem concerning electromagnetic casting of molten metals consists of looking for an electric current density distribution such that the induced electromagnetic field makes a given mass of liquid metal acquire a predefined shape. This problem is formulated here as an optimization problem where the positions of a finite set of inductors are the design variables. Two different formulations for this optimization problem for the two-dimensional case are proposed. The first one minimizes the difference between the target and the equilibrium shapes while the second approach minimizes the L^2 norm of a fictitious surface pressure that makes the target shape to be in mechanical equilibrium. The optimization problems are solved using Feasible Arc Interior Point Algorithm, a line search interior-point algorithm for nonlinear optimization. Some examples are presented to show the effectiveness of the proposed approaches.

Keywords Inverse problem · Free boundary · Electromagnetic shaping · Nonlinear optimization

A. Canelas (✉) · J. Herskovits
Mechanical Engineering Program, COPPE,
Federal University of Rio de Janeiro, P.O. Box 68503,
CEP 21945-970, CT, Cidade Universitária,
Ilha do Fundão, Rio de Janeiro, Brazil
e-mail: acanelas@optimize.ufrj.br

J. Herskovits
e-mail: jose@optimize.ufrj.br

J. R. Roche
I.E.C.N., CNRS, INRIA, Nancy-Université, B.P. 239,
54506 Vandoeuvre lès Nancy, France
e-mail: roche@iecn.u-nancy.fr

1 Introduction

Electromagnetic Casting (EMC) and Magnetic Suspension Melt Processing are very important technologies in the metallurgical industry. They make use of an electromagnetic field for contactless heating, shaping and control of solidification of hot melts. Advantages of these techniques are high surface quality, high cleanliness, low contamination and near-net shape manufacturing. The ECM has primarily been employed for containerless continuous casting but is mainly used to prepare ingots of aluminum alloy (Zhiqiang et al. 2002). Another important application, extensively used in aeronautics, astronautics, energy and chemical engineering, is in the manufacturing of components of engines made of superalloy materials (Ni,Ti,...) (Fu et al. 2004).

These technologies are based on the repulsive forces that an alternating electromagnetic field produces on the surface of this kind of materials. This electromagnetic field is induced by an externally imposed alternating current. Under suitable assumptions, the mathematical model is described by a set of equations expressing an equilibrium relation on the boundary between electromagnetic pressures and surface tensions, as well as gravity forces in the three-dimensional problem. The boundary shape of the liquid metal such that the equilibrium is attained can be found as the solution of a nonlinear free surface problem, see Pierre and Roche (1991, 1993) for details.

In this paper we study the electromagnetic shaping of a vertically falling molten metal column with a magnetic field induced by a set of vertical electric wires. Our problem consists of locating the wires in order to have an horizontal cross-section of the molten metal as

close as possible to a prescribed shape. Two different approaches are proposed, the first one looks for a set of inductors such that the distance between the computed shape and the given target one is minimized. In the second approach the error of the equilibrium equation for the target shape is minimized.

Simultaneous Analysis and Design optimization, SAND, is a formulation that includes the state variables as unknowns of the mathematical program and the state equations as equality constraints, see Haftka (1985), Haftka and Kamat (1989), Arora and Wang (2004, 2005), Herskovits et al. (2005), Canelas et al. (2007). In this paper we employ a SAND formulation for both approaches and solve the optimization problems employing the *Feasible Arc Interior Point Algorithm* (FAIPA), a line search interior-point algorithm for nonlinear optimization (Herskovits 1998; Herskovits et al. 2005, 1996).

2 The mathematical model of the electromagnetic shaping problem

The electromagnetic shaping problem studied here concerns a vertical column of liquid metal falling down into an electromagnetic field induced by vertical conductors. We consider a model for high frequencies of the imposed currents that assumes that the magnetic field does not penetrate into the metal. Thus, the electromagnetic forces are reduced to the magnetic pressure acting on the interface.

Let ω be the open and simply connected domain in the horizontal plane occupied by the liquid metal, $\Gamma = \partial\omega$ its boundary and $\Omega = \mathbb{R}^2 \setminus \bar{\omega}$ the exterior of the liquid metal. The exterior magnetic field can be found as the solution of the following boundary value problem:

$$\nabla \times \mathbf{B} = \mu_0 \mathbf{j}_0 \quad \text{in } \Omega, \tag{1}$$

$$\nabla \cdot \mathbf{B} = 0 \quad \text{in } \Omega, \tag{2}$$

$$\mathbf{B} \cdot \nu = 0 \quad \text{on } \Gamma, \tag{3}$$

$$\|\mathbf{B}\| = O(\|x\|^{-1}) \quad \text{as } \|x\| \rightarrow \infty \text{ in } \Omega. \tag{4}$$

Here the fields $\mathbf{j}_0 = (0, 0, j_0)$ and $\mathbf{B} = (B_1, B_2, 0)$ represent the mean square values of the current density vector and the total magnetic field, respectively. The constant μ_0 is the vacuum permeability, ν the unit normal vector to the boundary Γ and $\|\cdot\|$ denotes the Euclidean norm. We assume that j_0 has compact support in Ω and satisfies:

$$\int_{\Omega} j_0 \, dx = 0. \tag{5}$$

On the other hand, the magnetic field produces a surface pressure that acts on the liquid metal, changing the shape until the equilibrium is attained. This equilibrium is characterized by the following equation (Pierre and Roche 1991, 1993):

$$\frac{1}{2\mu_0} \|\mathbf{B}\|^2 + \sigma \mathcal{C} = p_0 \quad \text{on } \Gamma, \tag{6}$$

where \mathcal{C} is the curvature of Γ seen from the metal, σ is the surface tension of the liquid and the constant p_0 is an unknown of the problem. Physically, p_0 represents the difference between the internal and external pressures. Since it is assumed that the molten metal is incompressible, we have the following condition:

$$\int_{\omega} dx = S_0, \tag{7}$$

where S_0 is given.

In the direct problem the electric current density j_0 is given and one needs to find the shape of ω that satisfies (7) and such that the magnetic field \mathbf{B}_{ω} solution of (1)–(4) satisfies also the equilibrium equation (6) for a real constant p_0 .

Conditions (1)–(5), with the function j_0 compactly supported in Ω , imply that there exists a potential function $\varphi : \Omega \rightarrow \mathbb{R}$ such that $\mathbf{B} = (\frac{\partial\varphi}{\partial x_2}, -\frac{\partial\varphi}{\partial x_1}, 0)$ and φ is the solution of:

$$\begin{aligned} -\Delta\varphi &= \mu_0 j_0 \quad \text{in } \Omega, \\ \varphi &= 0 \quad \text{on } \Gamma, \\ \varphi(x) &= O(1) \quad \text{as } \|x\| \rightarrow \infty. \end{aligned} \tag{8}$$

The equilibrium equation (6) in terms of the potential φ becomes:

$$\frac{1}{2\mu_0} \|\nabla\varphi\|^2 + \sigma \mathcal{C} = p_0 \quad \text{on } \Gamma. \tag{9}$$

The direct problem, in terms of the potential, consists of looking for a domain ω such that the solution φ_{ω} of (8) satisfies (9) for a real constant p_0 .

2.1 The variational model of the direct problem

Under suitable assumptions, the equilibrium configurations are given by the local stationary points with respect to the domain of the following total energy:

$$E(\omega) = -\frac{1}{2\mu_0} \int_{\Omega} \|\nabla\varphi_{\omega}\|^2 \, dx + \sigma P(\omega), \tag{10}$$

subject to the equality constraint in the measure of ω :

$$\int_{\omega} dx = S_0. \tag{11}$$

In (10), φ_ω is the solution of (8) and $P(\omega)$ is the perimeter of ω , i.e., the length of $\Gamma = \partial\omega$ when $\partial\omega$ is regular enough (for instance of class C^1):

$$P(\omega) = \int_\Gamma d\Gamma, \quad d\Gamma = \text{length measure on } \Gamma. \quad (12)$$

The variational formulation of the direct problem consists of finding the domain ω as a stationary point of the total energy (10), subject to the constraint (11). As φ_ω is solution of (8), to prove that this variational formulation is equivalent to the previous one it remains to show that the equilibrium relation is automatically ensured for all the stationary points.

Theorem 1 *Let Ω be the complement of a compact set ω in \mathbb{R}^2 with nonempty interior. Assume that $\Gamma = \partial\omega$ is of class C^2 . Let V be in $C^1(\mathbb{R}^2, \mathbb{R}^2)$ with compact support and*

$$\forall x \in \mathbb{R}^2, \quad T_t x = x + tV(x) = (I + tV)(x), \quad (13)$$

$$\Omega_t = T_t(\Omega), \quad \partial\Omega_t = T_t(\partial\Omega) \quad (t \text{ small enough}). \quad (14)$$

Finally, let j_0 be a square integrable function from Ω into \mathbb{R} with compact support in Ω .

Then, for t small enough, there exists a unique solution φ_{ω_t} in $C^1(\overline{\Omega}_t)$ (see Kress 1999 and Henrot and Pierre 1989) of:

$$\begin{aligned} -\Delta\varphi_{\omega_t} &= \mu_0 j_0 \quad \text{in } \Omega_t, \\ \varphi_{\omega_t} &= 0 \quad \text{on } \partial\Omega_t, \\ \varphi_{\omega_t}(x) &= O(1) \quad \text{as } \|x\| \rightarrow \infty. \end{aligned} \quad (15)$$

Moreover, if

$$E(\omega_t) = -\frac{1}{2\mu_0} \int_{\Omega_t} \|\nabla\varphi_{\omega_t}\|^2 dx + \sigma P(\omega_t), \quad (16)$$

then, for all $p_0 \in \mathbb{R}$:

$$\begin{aligned} \frac{d}{dt} (E(\omega_t) - p_0 \text{mes}(\omega_t)) \Big|_{t=0} &= \\ &= \int_\Gamma \left(\frac{1}{2\mu_0} \|\nabla\varphi_{\omega_t}\|^2 + \sigma\mathcal{C} - p_0 \right) (V \cdot \nu) d\Gamma, \end{aligned} \quad (17)$$

where ν is the unit normal to Γ oriented toward Ω .

Proof see Henrot and Pierre (1989), Pierre and Roche (1991), Novruzi and Roche (1995). \square

This problem is very similar to some ones considered by several authors. We refer the readers to the following papers and references therein for the physical

analysis of the simplifying assumptions that the above model requires: see Brancher and Séro-Guillaume (1985), Coulaud and Henrot (1994), Gagnoud et al. (1986), Henrot and Pierre (1989), Henrot et al. (1989), Moffatt (1985), Novruzi (1997), Novruzi and Roche (1995, 2000), Pierre and Roche (1991, 1993), Roche (1996, 1997), Séro-Guillaume et al. (1992), Sneyd and Moffatt (1982), Zouaoui et al. (1990).

3 The inverse problem

The goal of the inverse problem is to find a distribution of current around the liquid metal column so that it attains a given shape.

Given the target shape ω^* , we want to compute j_0 solution of the following optimization problem:

$$\min_{j_0} d(\omega, \omega^*), \quad (18)$$

where the function d is a distance between ω and ω^* . The domain ω belongs to the set of admissible domains, i.e., $\omega \in \mathcal{O}$, and is in equilibrium under the action of the electric current density j_0 in the variational sense. In other words, ω satisfies the area constraint (11) and the potential φ_ω solution of (8) satisfies the equilibrium equation (19) for a real constant p_0 :

$$\begin{aligned} \int_\Gamma \left(\frac{1}{2\mu_0} \|\nabla\varphi_\omega\|^2 + \sigma\mathcal{C} - p_0 \right) (V \cdot \nu) d\Gamma &= 0 \\ \forall V \text{ in } C^1(\mathbb{R}^2, \mathbb{R}^2). \end{aligned} \quad (19)$$

From a practical point of view, the magnetic field has to be created by a simple configuration of inductors. For that purpose, we consider a distribution of the electric current density j_0 of the form:

$$j_0 = I \sum_{p=1}^m \alpha_p \delta_{x_p}, \quad (20)$$

where I is a given intensity of current, δ_{x_p} , with $1 \leq p \leq m$, are Dirac masses at points x_p in the plane, and α_p are dimensionless coefficients. Then, the inverse problem consists of determining the positions in the plane of the points x_p .

Remark 1 In certain cases it is possible to find a current density distribution such that the target shape ω^* is in equilibrium. This topic was already studied and there are a few papers about the existence of such solutions. See Henrot and Pierre (1989), Felici and Brancher (1991), Pierre and Rouy (1996).

In the two-dimensional case, ω^* is assumed simply connected and its boundary is only one Jordan curve Γ . Henrot and Pierre (1989), show that a solution of (1), (2), (3), (4), and (6), with j_0 compactly supported in Ω can be found for each p_0 satisfying:

$$p_0 \geq \sigma \max_{x \in \Gamma} \mathcal{C}(x), \tag{21}$$

That is, assuming j_0 compactly supported in Ω , and choosing p_0 satisfying (21), then there exists \mathbf{B} satisfying (1), (2), (3), (4), and (6) if and only if:

- (i) Γ is an analytic curve.
- (ii) If p_0 is chosen satisfying the equality in (21), the global maximum of the curvature must be attained in an even number of points.

Moreover, the magnetic field is well determined in a neighborhood of ω (local uniqueness).

Equation (5) is also obtained if p_0 is chosen satisfying the equality in (21). A current density distribution concentrated on a curve in Ω can always be found. However, a solution given by the addition of a finite number of Dirac masses is not always possible. See Henrot and Pierre (1989).

3.1 Two approaches for the inverse problem

We propose two different approaches for finding an approximate solution of problem (18). The first one considers a domain deformation of ω^* defined by the mapping:

$$T_Z(x) = x + Z(x), \quad \forall x \in \mathbb{R}^2, \tag{22}$$

where Z is a regular vector field with compact support in \mathbb{R}^2 . Then, defining:

$$\begin{aligned} \omega_Z &= T_Z(\omega^*), \\ \Gamma_Z &= T_Z(\Gamma^*). \end{aligned}$$

The first inverse formulation is:

$$\begin{aligned} &\min_{j_0, Z} \|Z\|_{L^2(\Gamma^*)}^2, \\ &\text{subject to:} \\ &\omega_Z \text{ is in equilibrium under } j_0. \end{aligned} \tag{23}$$

A second formulation of the inverse problem can be considered introducing a slack variable function $p(x) : \Gamma \rightarrow \mathbb{R}$ in order to make the equilibrium equation satisfied for the target shape:

$$\begin{aligned} &\int_{\Gamma^*} \left(\frac{1}{2\mu_0} \|\nabla \varphi_\omega\|^2 + \sigma \mathcal{C} - p_0 + p \right) (V \cdot \nu) d\Gamma = 0 \\ &\forall V \text{ in } C^1(\mathbb{R}^2, \mathbb{R}^2). \end{aligned} \tag{24}$$

The function p can be understood as an additional pressure acting on the interface. Given j_0 and ω^* , p is the surface pressure that equilibrates the action of the magnetic pressure and the surface tension. The second formulation for the inverse problem is an indirect approach that try to minimize the $L^2(\Gamma^*)$ norm of the function p :

$$\begin{aligned} &\min_{j_0, p} \|p\|_{L^2(\Gamma^*)}^2, \\ &\text{subject to:} \\ &\omega^* \text{ is in equilibrium under } j_0 \text{ and } p. \end{aligned} \tag{25}$$

Remark 2 There are not shape variables in this formulation. This fact makes (25) much easier to solve than (23). If the function p vanishes at the solution of (25), the resulting electric current density j_0 will also be a solution of the first formulation with the equilibrium domain matching exactly the target shape. In the general case, p will not vanish at the solution and, in this case, the target shape ω^* will not be in equilibrium under j_0 only. Then, a second stage of analysis will be necessary to find the equilibrium domain under the obtained current density distribution. However, as the norm of p was minimized, the resultant equilibrium domain is expected to be a good approximation of the target one. Furthermore, since (25) can be solved with a minor computational effort, its solution j_0 can be employed as an initial guess for the formulation (23).

4 Numerical method

4.1 The exterior Dirichlet problem

To solve (8) in the exterior domain Ω we consider a particular solution φ_1 of the differential equation given by:

$$\varphi_1(x) = -\frac{\mu_0}{2\pi} \int_{\mathbb{R}^2} \ln \|x - y\| j_0(y) dy. \tag{26}$$

This function is a solution of the problem:

$$-\Delta \varphi_1(x) = \mu_0 j_0 \quad \text{in } \mathbb{R}^2, \tag{27}$$

$$\varphi_1(x) = O(1) \quad \text{as } \|x\| \rightarrow \infty. \tag{28}$$

Note that for the current density distribution defined by (20), the expression of φ_1 is:

$$\varphi_1(x) = I \sum_{p=1}^m \alpha_p \ln \|x - x_p\|. \tag{29}$$

The function φ can be computed as:

$$\varphi(x) = v(x) + \varphi_1(x), \tag{30}$$

where the function v is the solution of the following exterior problem:

$$\begin{aligned} -\Delta v(x) &= 0 && \text{in } \Omega, \\ v(x) &= -\varphi_1(x) && \text{on } \Gamma, \\ \|v(x)\| &= O(1) && \text{as } \|x\| \rightarrow \infty. \end{aligned} \tag{31}$$

Following Kress (1999), an integral single layer representation of the solution of (31) is given by:

$$v(x) = -\frac{1}{2\pi} \int_{\Gamma} q(y) \ln \|x - y\| d\Gamma + c, \tag{32}$$

where the constant c is the value at the infinity of v and the function $q(y) \in H^{-1/2}(\Gamma)$ satisfies:

$$\int_{\Gamma} q(y) d\Gamma = 0. \tag{33}$$

It remains to impose the boundary conditions on Γ . Here, this is done with a weak formulation. Let $a_{\Gamma}(q, g)$ be the following elliptic bilinear form:

$$\begin{aligned} a_{\Gamma}(q, g) &= -\frac{1}{2\pi} \int_{\Gamma} g(x) \int_{\Gamma} q(y) \ln \|x - y\| d\Gamma d\Gamma + \\ &+ c \int_{\Gamma} g(x) d\Gamma \end{aligned} \tag{34}$$

defined on $H^{-1/2}(\Gamma) \times H^{-1/2}(\Gamma)$. We look for a function $q(y) \in H^{-1/2}(\Gamma)$ that satisfies (33) and:

$$a_{\Gamma}(q, g) = - \int_{\Gamma} \varphi_1(x)g(x) d\Gamma \quad \forall g \in H^{-1/2}(\Gamma). \tag{35}$$

Finally, the norm $\|\nabla\varphi\|$ in (19) can be computed as:

$$\|\nabla\varphi\| = \left| \frac{\partial\varphi}{\partial v} \right| = \left| \frac{\partial\varphi_1}{\partial v} + \frac{\partial v}{\partial v} \right|, \tag{36}$$

where the first equality comes from the fact that φ is constant on Γ , and the second one from (30). The normal derivative of φ_1 is obtained from (26):

$$\frac{\partial\varphi_1}{\partial v_x}(x) = -\frac{\mu_0}{2\pi} \int_{\mathbb{R}^2} \frac{\partial}{\partial v_x} \ln \|x - y\| j_0(y) dy. \tag{37}$$

The following expression can be used for v :

$$\begin{aligned} \frac{\partial v}{\partial v_x}(x) &= -\frac{1}{2\pi} \int_{\Gamma} q(y) \frac{\partial}{\partial v_x} \ln \|x - y\| d\Gamma \\ &+ \frac{1}{2}q(x) \quad \forall x \in \Gamma, \end{aligned} \tag{38}$$

where the integral of (38) is understood in the Cauchy principal value sense.

4.2 The SAND formulation of the inverse problems

A SAND formulation of the inverse problems (23) and (25) is employed here. In other words, the state variables p_0, c and q are incorporated as unknowns of the optimization problem and the state and equilibrium equations are incorporated as equality constraints. The optimization problem of the formulation (23) becomes:

$$\min_{j_0, Z, p_0, c, q} \|Z\|_{L^2(\Gamma^*)}^2, \tag{39}$$

subject to the area constraint:

$$\int_{\omega_Z} dx = S_0, \tag{40}$$

the state equations:

$$a_{\Gamma_Z}(q, g) = - \int_{\Gamma_Z} \varphi_1(x)g(x) d\Gamma \quad \forall g \in H^{-1/2}(\Gamma_Z), \tag{41}$$

$$\int_{\Gamma_Z} q(y) d\Gamma = 0, \tag{42}$$

and the equilibrium equation:

$$\begin{aligned} \int_{\Gamma_Z} \left(\frac{1}{2\mu_0} \|\nabla\varphi\|^2 + \sigma\mathcal{E} - p_0 \right) (V \cdot v) d\Gamma &= 0 \\ \forall V \text{ in } C^1(\mathbb{R}^2, \mathbb{R}^2), \end{aligned} \tag{43}$$

where φ_1, φ , and v are given by (26), (30) and (32).

The optimization problem of the formulation (25) becomes:

$$\min_{j_0, p, p_0, c, q} \|p\|_{L^2(\Gamma^*)}^2, \tag{44}$$

subject to the state equations:

$$a_{\Gamma^*}(q, g) = - \int_{\Gamma^*} \varphi_1(x)g(x) d\Gamma \quad \forall g \in H^{-1/2}(\Gamma^*), \tag{45}$$

$$\int_{\Gamma^*} q(y) d\Gamma = 0, \tag{46}$$

and the equilibrium equation:

$$\begin{aligned} \int_{\Gamma^*} \left(\frac{1}{2\mu_0} \|\nabla\varphi\|^2 + \sigma\mathcal{E} - p_0 + p \right) (V \cdot v) d\Gamma &= 0 \\ \forall V \text{ in } C^1(\mathbb{R}^2, \mathbb{R}^2). \end{aligned} \tag{47}$$

4.3 The numerical model

4.3.1 Discretization of the domain

We consider an approximation of the domain ω^* defined by the piecewise linear closed boundary Γ^h , i.e., Γ^h is the union of the n linear finite elements ℓ^j in \mathbb{R}^2 , $j \in \{1, \dots, n\}$. The nodes of the boundary Γ^h are denoted by x^i .

A direction $\hat{Z}^i \in \mathbb{R}^2$ is associated to each vertex x^i of Γ^h . We construct a continuous piecewise linear vector field Z^i from Γ^h in \mathbb{R}^2 such that $Z^i(x^k) = \delta_{ik} \hat{Z}^i$. The support of Z^i is equal to the union of the finite elements for which x^i is a node. The vector field Z of (22) is computed as:

$$Z(x) = \sum_{i=1}^n u_i Z^i(x), \tag{48}$$

and the updated boundary $\Gamma_{\mathbf{u}}$ is then given by:

$$\Gamma_{\mathbf{u}} = \{X \mid X = x + Z(x); u_i \in \mathbb{R}, x \in \Gamma^h\}, \tag{49}$$

where $\mathbf{u}^T = (u_1, \dots, u_n) \in \mathbb{R}^n$ is the vector of unknowns which determine the evolution of the boundary. This representation has the advantage of defining only one degree of freedom for each node. We denote by $\omega_{\mathbf{u}}$ the interior domain related to $\Gamma_{\mathbf{u}}$ in order to show the dependence with respect to the vector \mathbf{u} .

4.3.2 Exterior boundary value problem

For numerical calculations we consider a piecewise constant approximation $q_h(x)$ of $q(x)$:

$$q_h(x) = \sum_{j=1}^n q_j e_j(x), \tag{50}$$

where $e_j(x) = 1$ if $x \in \ell_j$ and zero elsewhere.

Replacing the function g in (41) by e_i , with $i \in \{1, \dots, n\}$, the weak formulation of the boundary value problem, given by equations (41) and (42), becomes:

$$\mathbf{A}(\mathbf{u})\mathbf{q} = \mathbf{b}(\mathbf{u}_p, \mathbf{u}), \tag{51}$$

where the vector $\mathbf{q}^T = (q_1, \dots, q_n, c)$ is in \mathbb{R}^{n+1} , \mathbf{u} is the vector of shape variables and \mathbf{u}_p is the vector that contains the coordinates of the positions of the inductors,

i.e. the coordinates of the points x_p with $p \in \{1, \dots, m\}$. The coefficients a_{ij} of the symmetric matrix $\mathbf{A}(\mathbf{u})$ are:

$$a_{ij}(\mathbf{u}) = -\frac{1}{2\pi} \int_{\ell_i} \int_{\ell_j} \ln \|x - y\| d\Gamma d\Gamma \quad i, j \in \{1, \dots, n\}, \tag{52}$$

$$a_{ij}(\mathbf{u}) = \int_{\ell_j} d\Gamma \quad i = n + 1, \text{ and } j \in \{1, \dots, n\}, \tag{53}$$

and the components b_i of the vector \mathbf{b} are:

$$b_i(\mathbf{u}_p, \mathbf{u}) = - \int_{\ell_i} \varphi_1(x) d\Gamma \quad i \in \{1, \dots, n\}, \tag{54}$$

$$b_i(\mathbf{u}_p, \mathbf{u}) = 0 \quad i = n + 1, \tag{55}$$

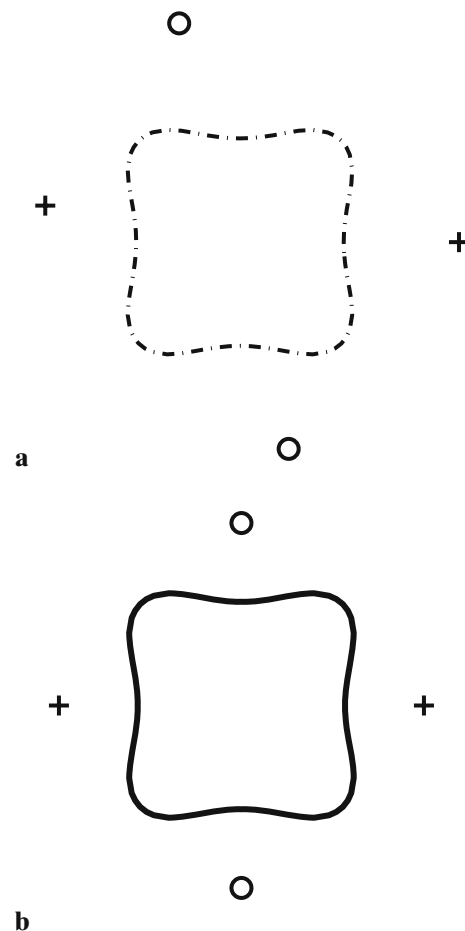


Fig. 1 Example 1a, configuration of inductors, **a** initial distribution, **b** final distribution. *Solid line*: equilibrium shape, *dash-dot line*: target shape, *plus*: positive current, *circle*: negative current

Remark 3 For given vectors \mathbf{u} and \mathbf{u}_p , the linear system (51) is symmetric and non-sparse. Numerical approximations of the element integrals of previous and later equations are computed by Gauss quadrature.

Remark 4 If q is the solution of the system (33), (35) and the piecewise constant approximation q_h given by the solution of (51), then we have the following error bounds, see Nédélec (1977):

$$\|q - q_h\|_{H^{-1/2}(\Gamma)} \leq C_1 h \|q\|_{H^1(\Gamma)}, \tag{56}$$

and if v_h is the approximation of (32) then

$$\left\| \frac{\partial v}{\partial \nu} - \frac{\partial v_h}{\partial \nu} \right\|_{H^{-1/2}(\Gamma)} \leq C_2 h \|q\|_{H^1(\Gamma)}. \tag{57}$$

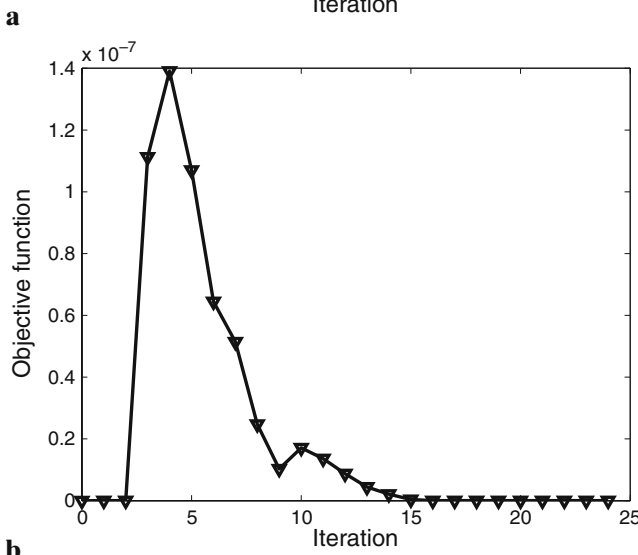
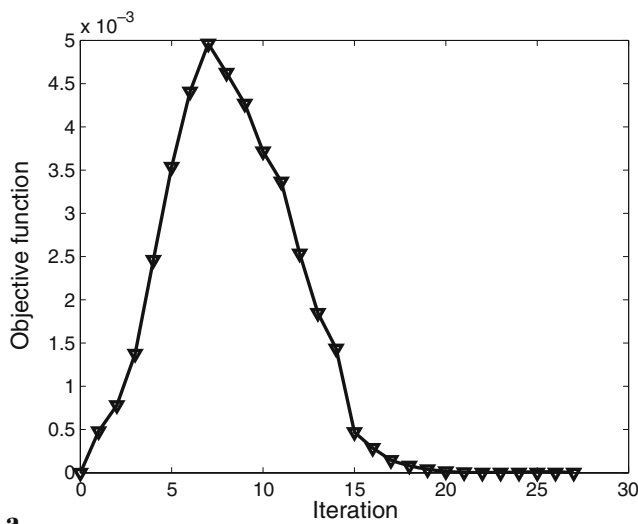


Fig. 2 Example 1a, evolution of the objective functions, **a** first formulation, **b** second formulation

Remark 5 The approximation of the normal derivative $\frac{\partial v}{\partial \nu}$ at $x_l \in \ell_l$ is given by:

$$\frac{\partial v_h}{\partial \nu}(x_l) = -\frac{1}{2\pi} \sum_{\substack{i=1 \\ i \neq l}}^n q_i \sum_{m=1}^K p_m \frac{\partial \ln \|x_l - x_i(s_m)\|}{\partial \nu} + \frac{1}{2} q_l, \tag{58}$$

where $x_i(s_m)$ are the integration points and p_m the weights of the Gauss quadrature formula. Thus, the computation of $\frac{\partial v_h}{\partial \nu}(x_l)$ needs $O(n)$ floating point operations.

4.3.3 Equilibrium equation

Consider a direction $\hat{V}^i \in \mathbb{R}^2$ associated to each vertex x^i of Γ^h and the continuous piecewise linear vector

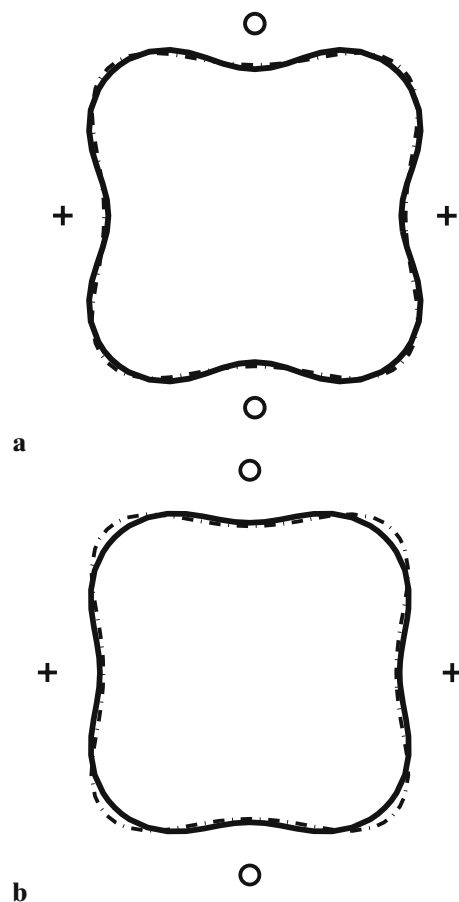


Fig. 3 Example 1b, configuration of inductors and final shape, **a** first formulation, **b** second formulation. *Solid line*: equilibrium shape, *dash-dot line*: target shape, *plus*: positive current, *circle*: negative current

field V^i from Γ^h in \mathbb{R}^2 such that $V^i(x^k) = \delta_{ik} \hat{V}^i$. If we project the equation (43) in the finite dimensional space generated by $V_i, i \in \{1, \dots, n\}$ the discrete version of the equilibrium is now the following:

$$DE_i(\mathbf{u}_p, \mathbf{u}, \mathbf{q}, p_0) = \int_{\Gamma_u} \left(\frac{1}{2\mu_0} \|\nabla\varphi\|^2 - p_0 \right) (V^i \cdot \nu) d\Gamma + \sigma \mathcal{C}^i \cdot \hat{V}^i, \tag{59}$$

where $i \in \{1, \dots, n\}$ and \mathcal{C}^i is an approximation of the mean curvature at x_i , given by:

$$\mathcal{C}^i = \left(\frac{(x_i - x_{i-1})}{\|x_i - x_{i-1}\|} - \frac{(x_{i+1} - x_i)}{\|x_{i+1} - x_i\|} \right). \tag{60}$$

The gradient $\nabla\varphi$ is computed using (36), (37) and (38).

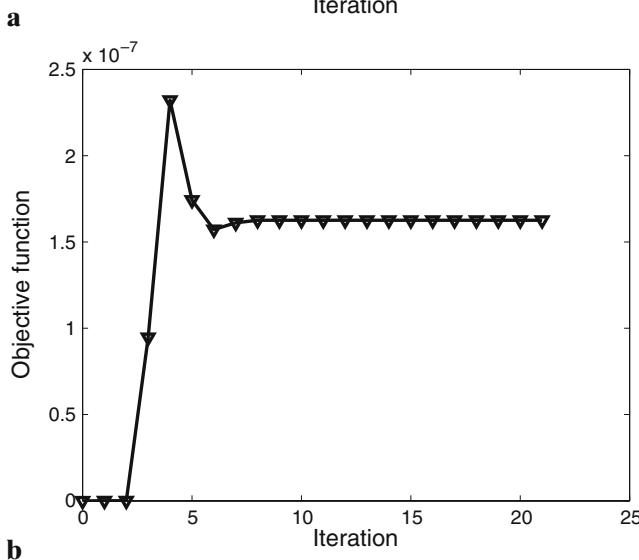
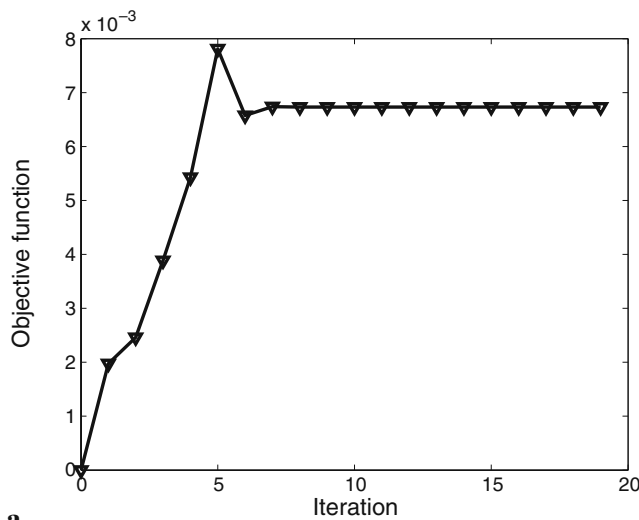


Fig. 4 Example 1b, evolution of the objective functions, **a** first formulation, **b** second formulation

In the case of equation (47), we consider a piecewise linear function p_h defined as:

$$p_h(x) = \sum_{i=1}^n p_i f_i, \tag{61}$$

where the function f_i satisfies $f_i(x_k) = \delta_{ik}$. Then, defining $\mathbf{p}^T = (p_1, \dots, p_n)$, the equilibrium equation is defined as:

$$DF_i(\mathbf{u}_p, \mathbf{p}, \mathbf{q}, p_0) = \frac{1}{2\mu_0} \int_{\Gamma^*} (\|\nabla\varphi\|^2 - p_0 + p_h) (V^i \cdot \nu) d\Gamma + \sigma \mathcal{C}^i \cdot \hat{V}^i. \tag{62}$$

4.4 Discretized inverse problems

Let the area function be $S(\mathbf{u}) = \int_{\omega_u} dx$, and $DE(\mathbf{u}_p, \mathbf{u}, \mathbf{q}, p_0)$ the vector function such that $(DE)_i = DE_i(\mathbf{u}_p,$

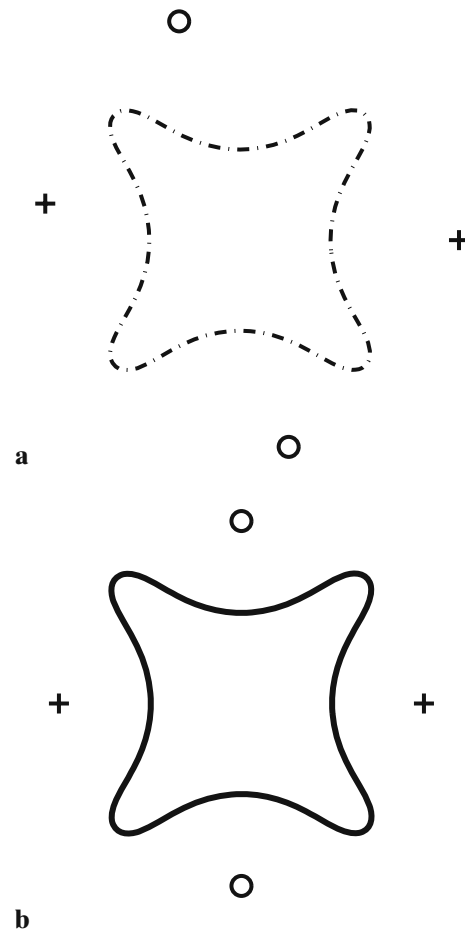


Fig. 5 Example 2a, configuration of inductors, **a** initial distribution, **b** final distribution. *Solid line*: equilibrium shape, *dash-dot line*: target shape, *plus*: positive current, *circle*: negative current

$\mathbf{u}, \mathbf{q}, p_0$). The discretized version of the first inverse problem is the following:

$$\min_{\mathbf{u}_p, \mathbf{u}, \mathbf{q}, p_0} \|Z\|_{L^2(\Gamma^*)}^2, \tag{63}$$

subject to the nonlinear equality constraints:

$$\begin{pmatrix} \mathbf{A}(\mathbf{u})\mathbf{q} - \mathbf{b}(\mathbf{u}_p, \mathbf{u}) \\ S(\mathbf{u}) - S_0 \\ DE(\mathbf{u}_p, \mathbf{u}, \mathbf{q}, p_0) \end{pmatrix} = 0. \tag{64}$$

The discretized version of the second inverse problem is:

$$\min_{\mathbf{u}_p, \mathbf{q}, c, p_0} \|p\|_{L^2(\Gamma^*)}^2, \tag{65}$$

with the constraint:

$$\begin{pmatrix} \mathbf{A}\mathbf{q} - \mathbf{b}(\mathbf{u}_p) \\ DF(\mathbf{u}_p, \mathbf{p}, \mathbf{q}, p_0) \end{pmatrix} = 0. \tag{66}$$

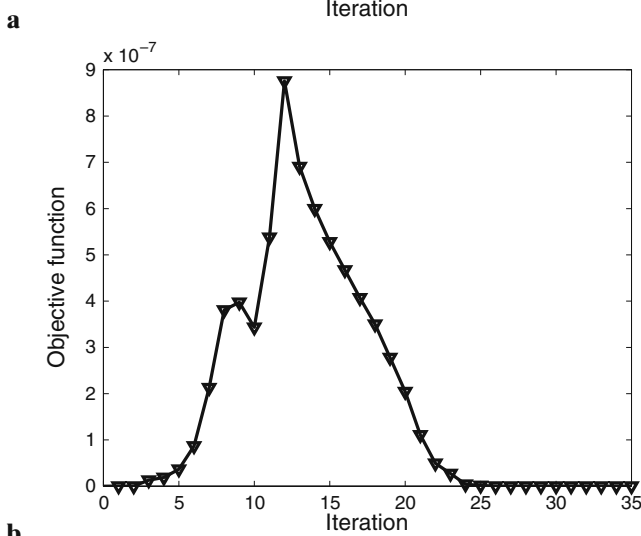
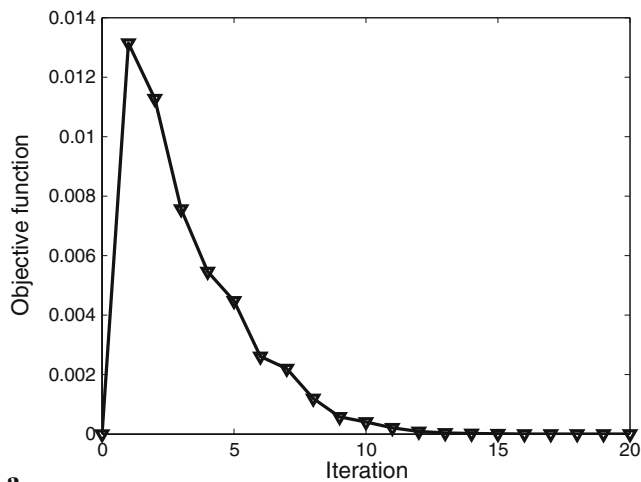


Fig. 6 Example 2a, evolution of the objective functions, **a** first formulation, **b** second formulation

In this case, since the integrals are defined on the fixed domain Γ^* the vector \mathbf{u} of shape variables is not present in the formulation.

5 Numerical examples

We consider seven examples to illustrate the behavior of the proposed formulations of the inverse problem. The goal is to identify the position of the inductors given by the points x_p of equation (20). The shape and the surface S_0 of the target shape, the surface tension σ , the intensity I and the dimensionless coefficients α_p are given. The initial values of the state variables \mathbf{q} and p_0 , the shape variable \mathbf{u} of the first formulation and the pressure \mathbf{p} of the second one are set equal to zero for all the examples.

For the solution of the optimization problems, the line search interior-point algorithm for nonlinear constrained optimization problems FAIPA was employed.

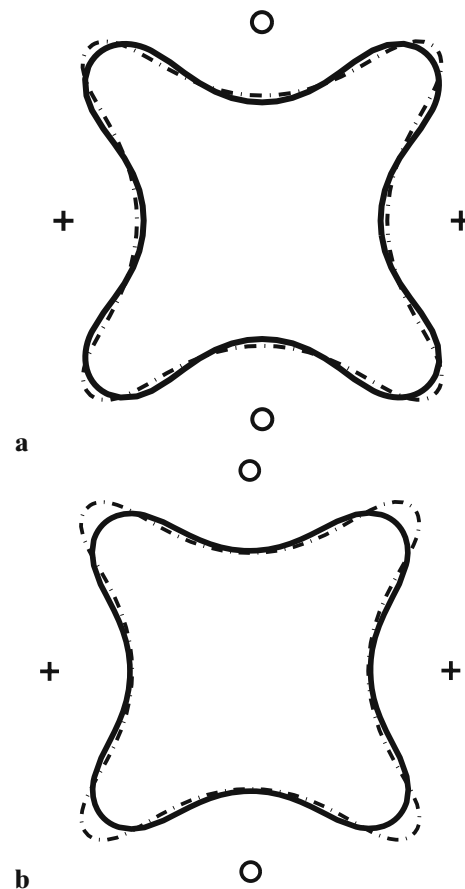


Fig. 7 Example 2b, configuration of inductors and final shape, **a** first formulation, **b** second formulation. *Solid line*: equilibrium shape, *dash-dot line*: target shape, *plus*: positive current, *circle*: negative current

For a given feasible point with respect to the inequality constraints, FAIPA defines a feasible and descent arc solving three linear systems of equations with the same coefficient matrix. Then, it performs a line search along this arc to define the next iterate. FAIPA makes subsequent iterations until a certain convergence criterion is satisfied. For more details about FAIPA see Herskovits (1998), Herskovits et al. (2005, 1996). Some box constraints were applied to the variables related to the inductor positions to prevent the inductors from penetrating the liquid metal or going to infinite. Box constraints can be included easily and are handled efficiently by FAIPA.

For each example we plot the initial position of the inductors, the initial shape, the final shape and the evolution of the objective function during the iterative process.

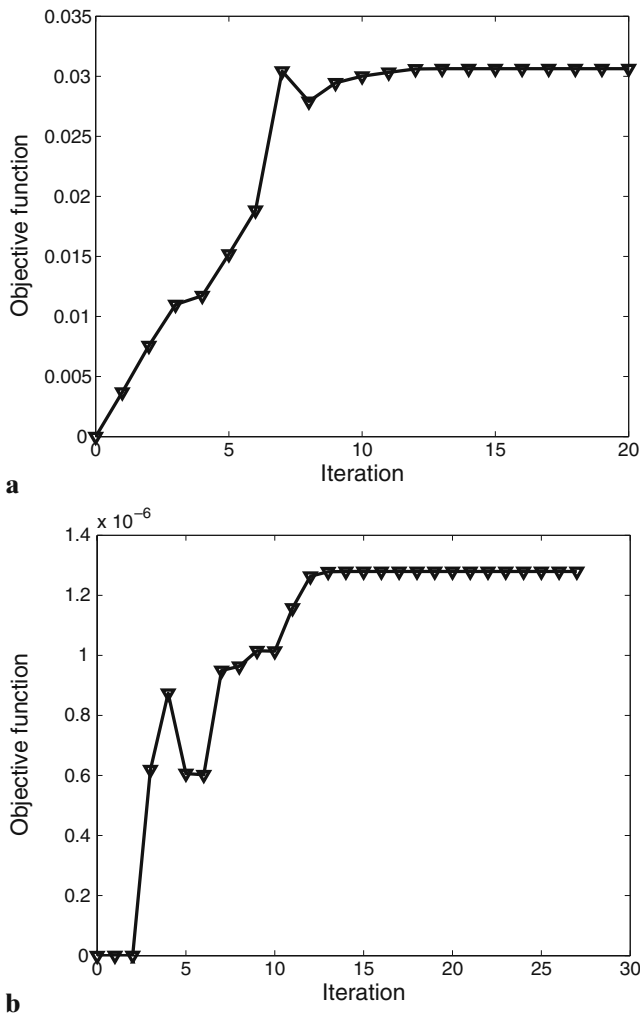


Fig. 8 Example 2b, evolution of the objective functions, **a** first formulation, **b** second formulation

5.1 Example 1a

In the first example we consider four inductors and a target shape of area S_0 equal to π . The intensity I is equal to 0.1 and the surface tension σ is equal to 1.0×10^{-4} . The dimensionless coefficients α_p have absolute value equal to 1.0 with the sign given by Fig. 1.

For validation purposes, the target shape considered in this example is the solution of the direct free-surface problem for known positions of the inductors. After the free-surface analysis, we consider the obtained shape as the target one for the inverse problem and perturb the position of the inductors. Then, the two formulations of the inverse problem have known solutions with zero value of the objective function.

Figure 1a depicts the initial positions of the inductors and the target shape. The final positions of the inductors are shown by Fig. 1b. In this example both formulations give the same positions for the inductors coinciding with the known solution.

Figure 2 shows the evolution of the objective function during the iterative process. The objective functions of both formulations vanish in the beginning due to the choice of the initial values of vectors \mathbf{u} and \mathbf{p} . Then, as the equality constraints are not satisfied, the expected behavior in the initial iterations is to

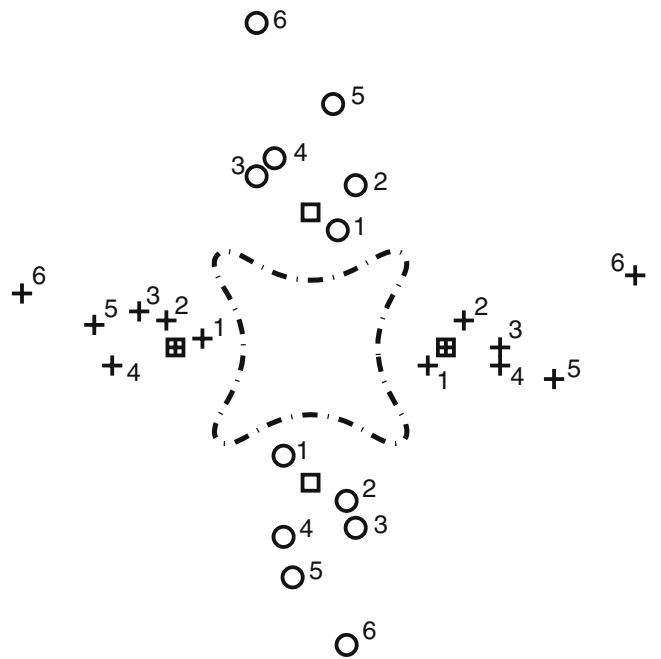


Fig. 9 Examples 2c1 to 2c6, target shape and initial configuration of inductors. 1: Example 2c1, 2: Example 2c2, 3: Example 2c3, 4: Example 2c4, 5: Example 2c5, 6: Example 2c6. *Dash-dot line*: target shape, *plus*: positive current, *circle*: negative current, *square*: position of the inductor at the solution

Table 1 Summary of results

Example ^a	Nodes	Inductors	Iterations	Objective ^b
Ex1a - F1	72	4	27	2.403e-013
Ex1a - F2	72	4	24	1.785e-017
Ex1b - F1	72	4	19	6.745e-003
Ex1b - F2	72	4	21	2.261e-002
Ex2a - F1	120	4	20	2.181e-013
Ex2a - F2	120	4	35	2.889e-015
Ex2b - F1	120	4	20	3.020e-002
Ex2b - F2	120	4	27	8.831e-002
Ex2c1 - F1	120	4	31	9.695e-014
Ex2c2 - F1	120	4	24	2.257e-014
Ex2c3 - F1	120	4	37	9.402e-014
Ex2c4 - F1	120	4	34	2.335e-013
Ex2c5 - F1	120	4	Fail	–
Ex2c6 - F1	120	4	Fail	–
Ex2c1 - F2	120	4	28	7.999e-015
Ex2c2 - F2	120	4	31	3.955e-016
Ex2c3 - F2	120	4	27	3.314e-015
Ex2c4 - F2	120	4	30	8.384e-015
Ex2c5 - F2	120	4	38	6.908e-013
Ex2c6 - F2	120	4	110	1.895e-014
Ex3 - F1	136	36	400	1.102e-004
Ex3 - F2	136	36	192	3.206e-003
Ex4 - F1	152	48	400	6.192e-003
Ex4 - F2	152	48	400	1.713e+000

^aF1: first formulation, F2: second formulation.
^bResult for the objective function of the first formulation.

increase the value of the objective function. After some iterations the values of the objective function reach a maximum and decrease in subsequent iterations. At the end of the iterative process the objective function reaches the optimum value and the equality constraints are satisfied.

5.2 Example 1b

In the second example we change only the intensity value to $I = 0.04$. This new value is smaller than the one used in the previous example. Then, the inductors will locate closer to the liquid metal than in Example 1a. Using the first formulation the algorithm does not find the exact target shape and using the second one it does not obtain the equilibrium. That means, probably, that

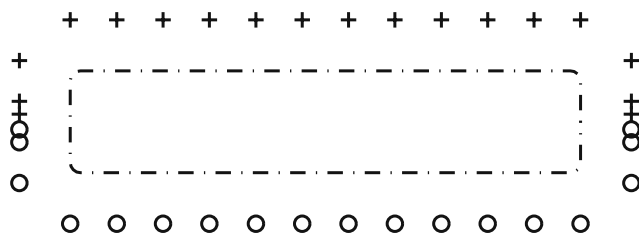


Fig. 10 Example 3, target shape and initial configuration of inductors

the target shape is not exactly shapable for a current distribution of the form given by (20).

Figure 3a shows the obtained shape and the positions of the inductors using the first formulation. Figure 3b depicts the same employing the second formulation.

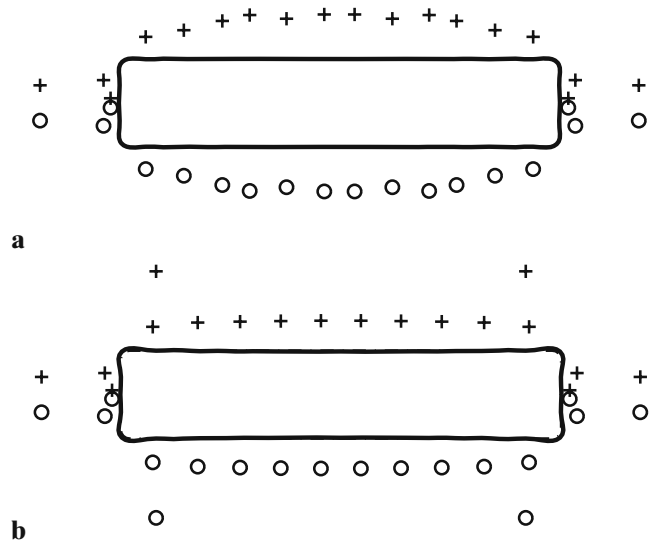


Fig. 11 Example 3, final configuration of inductors and final shape, **a** first formulation, **b** second formulation. *Solid line*: equilibrium shape, *dash-dot line*: target shape, *plus*: positive current, *circle*: negative current

The equilibrium shape in Fig. 3b represents the solution of the direct free-surface problem for the obtained configuration of inductors. Figure 4 shows the evolution of the objective function throughout the iterative process.

5.3 Example 2a

In this example, as in Example 1a, the target shape is the solution of a given direct problem for the same configuration of inductors but for an intensity factor $I = 0.2$. As in the Example 1a the obtained positions of the inductors match exactly the known ones. Figure 5 portrays the initial configuration of inductors, the target shape and the results for both formulations. Figure 6 shows the evolution of the objective function throughout the optimization process.

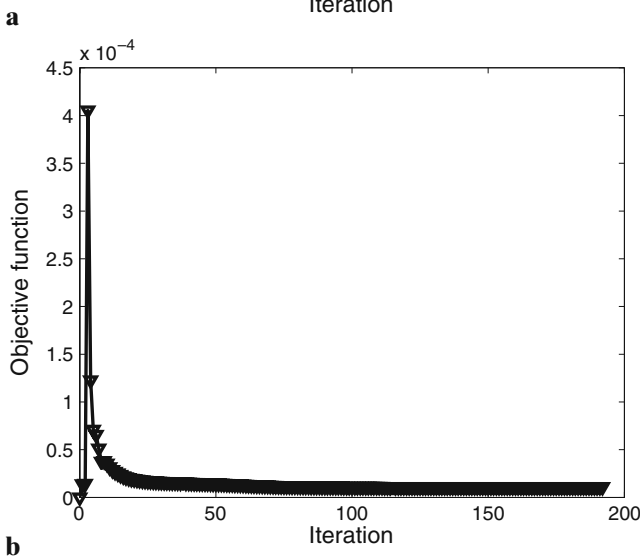
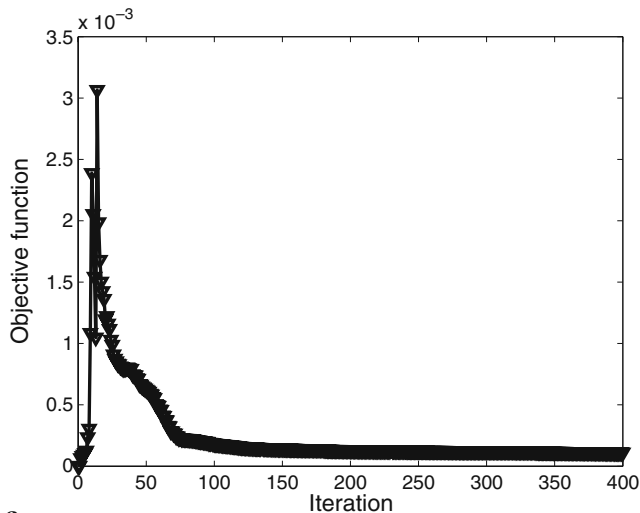


Fig. 12 Example 3, evolution of the objective functions, **a** first formulation, **b** second formulation

5.4 Example 2b

Here we change only the intensity value to $I = 0.1$. As this value is smaller than the considered before, the final positions of the inductors are closer to the liquid metal than in Example 2a. Like in Example 1b the first formulation does not obtain the target shape and the second one does not equilibrate exactly the target shape. Again, the target shape is probably not shapable for the distribution of electric current in the form given by (20).

Figure 7 shows the obtained results for this example. The evolution of the objective function throughout the iterative process is shown by Fig. 8.

5.5 Examples 2c1 to 2c6

In this example we consider the same parameters and target shape of the Example 2a. Six configurations for the initial positions of the inductors are considered to investigate the stability of the proposed formulations, see Fig. 9. For these examples, the initial inductors were located around the initial configuration of Example 2a. In the case of the Example 2c1 the inductors were located closer to the liquid metal than the Example 2a and also closer than the known solution. Examples 2c4 to 2c6 present initial inductors farther to the liquid metal than Example 2a. Table 1 shows that for Examples 2c1 to 2c4 both formulations converges to the known solution shown by Fig. 9 in a similar number of iterations. In examples 2c5 to 2c6 convergence to the solution is achieved only for the second formulation.

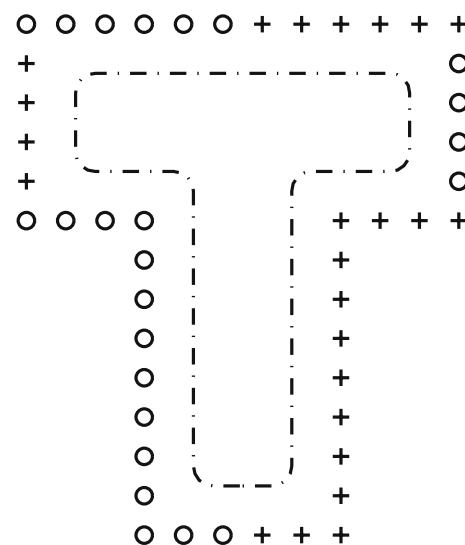


Fig. 13 Example 4, Target shape and initial configuration of inductors

5.6 Example 3

In this example we want to obtain a distribution of inductors in order to build a bar with rectangular cross-section. We consider thirty-six inductors and a surface S_0 equal to 4.98. The intensity is $I = 0.075$ and the surface tension σ is equal to 1.0×10^{-4} . The coefficients $\alpha_p = \pm 1$ with the sign given by Fig. 10.

Figure 11 portrays the obtained positions of the inductors for the two formulations of the inverse problem. The equilibrium shape in the Fig. 11b represents

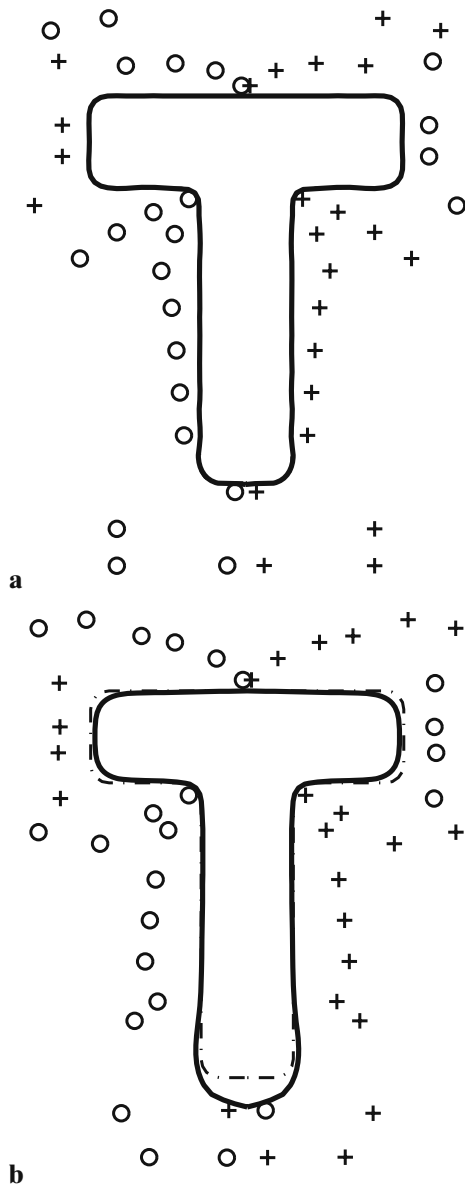


Fig. 14 Example 4, final distribution of inductors and final shape, **a** first formulation, **b** second formulation. *Solid line*: equilibrium shape, *dash-dot line*: target shape, *plus*: positive current, *circle*: negative current

the solution of the direct free-surface problem for the obtained configuration of inductors. Figure 12 shows the evolution of the objective function throughout the iterative process.

5.7 Example 4

This final example considers forty-eight inductors and the target shape of surface S_0 equal to 30.0 shown by Fig. 13. The intensity factor is $I = 0.03$ and the surface tension is $\sigma = 1.0 \times 10^{-4}$. The coefficients $\alpha_p = \pm 1$, with the sign given by Fig. 13.

Figure 14 depicts the obtained position of the inductors employing the two formulations of the inverse problem. Figure 15 shows the evolution of the objective functions during the optimization process.

Table 1 resumes the information about the considered examples. For each one we give the number of

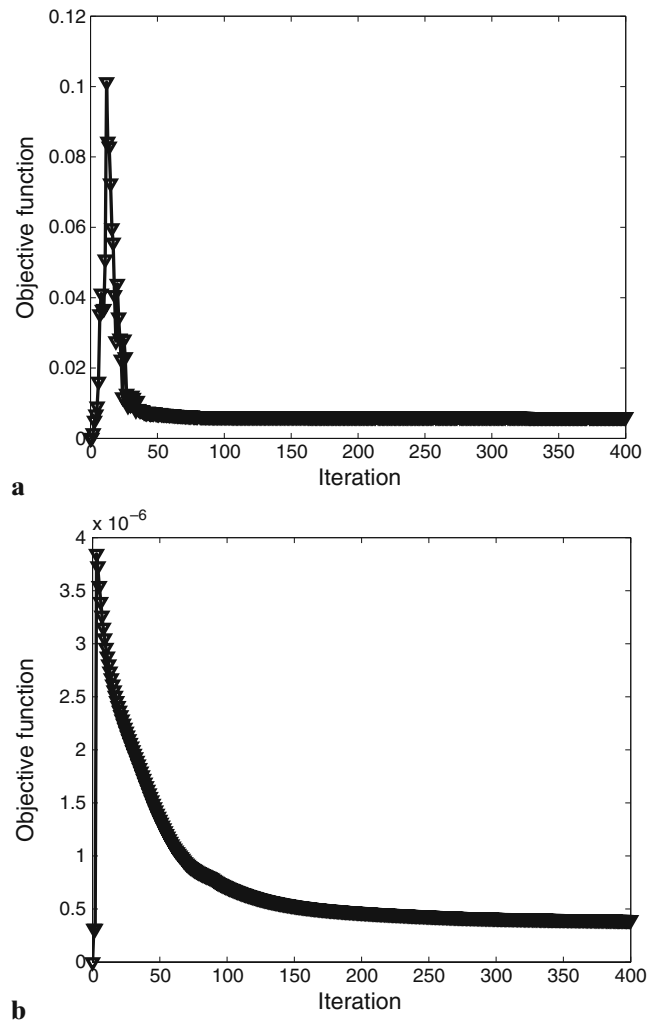


Fig. 15 Example 4, evolution of the objective functions, **a** first formulation, **b** second formulation

nodes used for the finite element approximation of the boundary Γ^* of the target shape, the number of inductors, the number of iterations performed by the optimization algorithm and the final value of the objective function. Table 1 shows that the total number of iterations is similar for both formulations in all the examples except for Example 4 for which the number of required iterations by the first formulation was smaller than the required by the second one. For comparison purposes, the value of the objective function of the first formulation is given in Table 1. As one could expect, the first formulation shows smaller values of the objective function in all the examples. The main advantage of the second formulation is that it gives similar results than the first one with a smaller computational cost since no variables related to the shape are present.

6 Conclusions

This paper studies an inverse problem concerning electromagnetic shaping of molten metals. Two different approaches based on nonlinear optimization has been proposed in order to find the positions of a suitable finite set of inductors for the two-dimensional case: the first one minimizes the difference between the geometries of the best possible equilibrium domain and the target shape; the second formulation minimizes a slack variable function related to the equilibrium equation on the target boundary.

The finite dimensional optimization problems obtained after discretization were solved employing the line search interior-point algorithm FAIPA.

Some presented examples show that both formulations are suitable for finding appropriate positions for the inductors. The main comments about them are: The first formulation found the best solutions in the entire set of examples. The second one leads to a simpler and less time consuming computation of the function derivatives because of the lack of shape variables. As it found relatively good results, this last formulation appear to be attractive for finding a first workable solution that can, if necessary, be improved in a later process employing it as an initial guess for the first formulation.

References

- Arora JS, Wang Q (2004) Optimization of large-scale structural systems using sparse SAND formulations. Tech. rep., Optimal Design Lab/CCAD, College of Engineering/4110 SC, The University of Iowa, Iowa City, IA 52242
- Arora JS, Wang Q (2005) Review of formulations for structural and mechanical system optimization. *Struct Multidisc Optim* 30(4):251–272
- Brancher JP, Séro-Guillaume OE (1985) Étude de la déformation d'un liquide magnétique. *Arch Ration Mech Anal* 90(1):57–85
- Canelas A, Herskovits J, Telles JCF (2007) Shape optimization using the boundary element method and a SAND interior point algorithm for constrained optimization. *Comput Struct* 86(13–14):1517–1526
- Coulaud O, Henrot A (1994) Numerical approximation of a free boundary problem arising in electromagnetic shaping. *SIAM J Numer Anal* 31(4):1109–1127
- Felici TP, Brancher JP (1991) The inverse shaping problem. *Eur J Mech B Fluids* 10(5):501–512
- Fu HZ, Shen J, Liu L, Hao QT, Li SM, Li JS (2004) Electromagnetic shaping and solidification control of Ni-base superalloys under vacuum. *J Mater Process Technol* 148(1):25–29
- Gagnoud A, Etay J, Garnier M (1986) Le problème de frontière libre en lévitation électromagnétique. *J Méc Théor Appl* 5(6):911–934
- Haftka RT (1985) Simultaneous analysis and design. *AIAA J* 23(7):1099–1103
- Haftka RT, Kamat MP (1989) Simultaneous nonlinear structural analysis and design. *Comput Mech* 4(6):409–416
- Henrot A, Pierre M (1989) Un problème inverse en formage de métaux liquides. *Modél Math Anal Numér* 23(1):155–177
- Henrot A, Brancher JP, Pierre M (1989) Existence of equilibria in electromagnetic casting. In: *Proceedings of the fifth international symposium on numerical methods in engineering*, vol. 1, 2 (Lausanne, 1989). *Computational Mechanics*, Southampton, pp 221–228
- Herskovits J (1998) Feasible direction interior-point technique for nonlinear optimization. *J Optim Theory Appl* 99(1):121–146
- Herskovits J, Laporte E, Le Tallec P, Santos G (1996) A quasi-Newton interior point algorithm applied to constrained optimum design in computational fluid dynamics. *Rev Européenne Éléme Finis* 5(5–6):595–617
- Herskovits J, Mappa P, Goulart E, Mota Soares CM (2005) Mathematical programming models and algorithms for engineering design optimization. *Comput Methods Appl Mech Eng* 194(30–33):3244–3268
- Kress R (1999) *Linear integral equations*. Applied mathematical sciences, vol 82, 2nd edn. Springer, New York
- Moffatt HK (1985) Magnetostatic equilibria and analogous Euler flows of arbitrarily complex topology. I. Fundamentals. *J Fluid Mech* 159:359–378
- Nédélec JC (1977) Approximation des équations intégrales en mécanique et en physique. Tech. rep., Centre de mathématiques appliquées -Ecole Polytechnique
- Novruzi A (1997) Contribution en optimisation de formes et applications. PhD thesis, Université Henri Poincaré, Nancy 1
- Novruzi A, Roche JR (1995) Second order derivatives, Newton method, application to shape optimization. Tech. Rep. RR-2555, INRIA
- Novruzi A, Roche JR (2000) Newton's method in shape optimization: a three-dimensional case. *BIT* 40(1):102–120
- Pierre M, Roche JR (1991) Computation of free surfaces in the electromagnetic shaping of liquid metals by optimization algorithms. *Eur J Mech B Fluids* 10(5):489–500
- Pierre M, Roche JR (1993) Numerical simulation of tridimensional electromagnetic shaping of liquid metals. *Numer Math* 65(2):203–217
- Pierre M, Rouy E (1996) A tridimensional inverse shaping problem. *Comm Partial Differ Equ* 21(7–8):1279–1305

- Roche JR (1996) Algorithmes numériques en optimization de formes et électromagnétisme, mémoire d'Habilitation à Diriger des Recherches
- Roche JR (1997) Gradient of the discretized energy method and discretized continuous gradient in electromagnetic shaping simulation. *Appl Math Comput Sci* 7(3):545–565
- Séro-Guillaume OE, Zouaoui D, Bernardin D, Brancher JP (1992) The shape of a magnetic liquid drop. *J Fluid Mech* 241:215–232
- Sneyd AD, Moffatt HK (1982) Fluid dynamical aspects of the levitation-melting process. *J Fluid Mech* 117:45–70
- Zhiqiang C, Fei J, Xingguo Z, Hai H, Junze J (2002) Microstructures and mechanical characteristics of electromagnetic casting and direct-chill casting 2024 aluminum alloys. *Mater Sci Eng A* 327(2):133–137
- Zouaoui D, Séro-Guillaume OE, Brancher JP (1990) Equilibrium of a magnetic liquid drop: variational approach and computation. *Magn Hidrodin* (4):32–35, 150